Polarimetric Camera Calibration Using an LCD Monitor

Zhixiang Wang[1] Yinqiang Zheng[2*] Yung-Yu Chuang[1]

[1]National Taiwan University [2]National Institute of Informatics

Abstract

It is crucial for polarimetric imaging to accurately calibrate the polarizer angles and the camera response function (CRF) of a polarizing camera. When this polarizing camera is used in a setting of multiview geometric imaging, it is often required to calibrate its intrinsic and extrinsic parameters as well, for which Zhang's calibration method is the most widely used with either a physical checker board, or more conveniently a virtual checker pattern displayed on a monitor. In this paper, we propose to jointly calibrate the polarizer angles and the inverse CRF (ICRF) using a slightly adapted checker pattern displayed on a liquid crystal display (LCD) monitor. Thanks to the lighting principles and the industry standards of the LCD monitors, the polarimetric and radiometric calibration can be significantly simplified, when assisted by the extrinsic parameters estimated from the checker pattern. We present a simple linear method for polarizer angle calibration and a convex method for radiometric calibration, both of which can be jointly refined in a process similar to bundle adjustment. Experiments have verified the feasibility and accuracy of the proposed calibration method.

1. Introduction

Polarization of a beam of light reflected from a surface conveys information about the azimuth and zenith angles, which can be used to determine the surface normal [8]. Surface reconstruction based on this principle is known as shape from polarization (SfP) [31, 25, 27, 6, 33, 41]. Compared to multi-view stereo methods, SfP has the advantage of independence from discriminative surface texture, and can be extended to reconstruct transparent objects [31, 25] or challenging dielectric objects [27, 6]. To capture polarimetric information, one can use a commodity polarizing camera [1, 2, 3], or conveniently construct a prototype by attaching a linear polarizer onto an ordinary camera, like a DLSR camera or an embedded camera in the mobile device.

To precisely estimate the surface normal using polarization, it is required to calibrate the camera response function (CRF) and the rotation angles of the polarizer. To control the exposure allows to calibrate the CRF, or equivalently the inverse CRF (ICRF), and to use a mechanical rotator can determine the polarizer angles, both of which are not always accessible. On the contrary, image-based self-calibration methods are more convenient in use, yet they usually suffer from issues in applicability and reliability. For example, the state-of-the-art self-calibration methods [32, 36] can estimate polarizer angles of a camera with linear/nonlinear response respectively. However, these methods require four and more polarizer angles, and thus do not work for polarizing cameras with no more than three polarizing channels, such as the FluxData camera [2]. As for reliability, their alternating optimization scheme depends on a good angle initialization for convergence, which is not always available. Also, when the CRF is nonlinear, the estimated angles will be severely distorted, unless an additional radiometric calibration method [35, 11, 28] is used beforehand to correct the image intensity. Therefore, a general, reliable and convenient method for radiometric and polarimetric calibration is needed.

Recently, polarization has been combined with other imaging modalities, such as depth sensors [15], binocular stereo [7] and multiview stereo [26, 9], because of their complementary characteristics. It requires to calibrate the camera's intrinsic and extrinsic parameters as well. Zhang's calibration method [43] is arguably the most widely used for this purpose, because of its proper tradeoff between the calibration accuracy and the difficulty in making a calibration target. Rather than using a physical checker board, some researches [14, 42, 34, 19] proposed to use a virtual checker pattern on a monitor, not only because of the easy availability of monitors, but also the augmented performance arising from monitor's properties. Given the popularity of geometric camera calibration using a checker pattern displayed on a monitor, a radiometric and polarimetric calibration method using similar calibration setup for a polarizing camera is likely to be widely used in practice.

In this paper, we first propose to calibrate the polarizer angles using the standard checker pattern displayed on a liquid crystal display (LCD) monitor. When the CRF is unknown,

*Corresponding Author, E-mail: yqzheng@nii.ac.jp

we jointly calibrate the ICRF and the polarizer angles using a slightly adapted checker pattern. Compared with existing self-calibration methods [32, 36], our method is greatly simplified, thanks to the extrinsic parameters obtained from the checker pattern, and to the lighting mechanisms and the industry standards of LCDs. Specifically, the relative in-plane rotation between the camera polarizer and the front polarizer of the monitor can be directly obtained by factorizing the extrinsic parameters of the checker pattern. In addition, the transmitted light from an LCD monitor is completely polarized, and an LCD monitor usually has a gamma of 2.2 under various display modes. The facts that transmitted light from an LCD monitor is highly polarized and the phase shift can be determined by extrinsic geometric parameter decomposition lead to a simple linear calibration method for the polarizer angles, which is applicable to cameras with two or more polarizing channels, less than four or more channels required in [32, 36]. The prior information on the LCD monitor gamma allows us to produce linear radiance by adapting the checker pattern, and the ICRF estimation boils down to a constrained parametric fitting problem, which is a convex quadratic program (QP).

Similar to bundle adjustment (BA) in geometric calibration, we jointly polish the ICRF and the polarizer angle estimation to account for imperfections in LCD gamma compensation. Experimental results have demonstrated the accuracy of our calibration method. Considering that LCD monitors are everywhere, we believe that our method is as easy to use as self-calibration methods, yet it is superior in application scope and reliability. In particular, it is suited for multi-view/multi-modality polarimetric imaging, as a by-product of geometric camera calibration.

2. Related Work

Polarization imaging. The polarization state of reflected light from a surface illuminated by unpolarized light encodes the surface normal information, which can be used to recover the surface geometry. This property has aroused intensive research efforts in shape from polarization [31, 25, 27, 6, 33, 41]. To correctly estimate the phase angle and the polarization status of the surface point, it is necessary to calibrate the ICRF and the polarizer angles of the camera.

Considering that polarization imaging has less restrictions on the illumination distribution and the surface reflectance properties, it has recently been used in conjunction with depth sensors [15], binocular stereo [7] and multiview stereo [26, 9]. SfP benefits from these modalities to resolve the ambiguity in azimuth angle estimation. In turn, polarization provides dense normal information that can be used to improve surface estimation, even with sparsely located texture. In addition to radiometric and polarimetric calibration, to merge polarization into other modalities requires to calibrate the camera intrinsic and extrinsic parameters.

Polarizer angle calibration. An ideal method for polarizer angle calibration is to use a mechanical rotator. However, most people do not possess such a specialized device. Schechner [32] proposed a self-calibration method, which applies only to a polarizing camera with four and more polarizing channels. The iterative algorithm is sensitive to initialization. It also assumes that the camera response is linear. When the camera indeed has nonlinear response, a third-party radiometric calibration method has to be used before conducting angle calibration. Teo *et al*. [36] proposed to estimate the nonlinear CRF and polarizer angles simultaneously. But the involvement of CRF estimation makes polarizer angle calibration less accurate. Besides, it requires more polarizer angles and is more sensitive to initialization.

Radiometric calibration. Radiometric calibration has been studied extensively in photometric computer vision, where the mapping between the irradiance and the recorded intensity is important. The response can be calibrated by controlling exposures [10, 24]. When there is no access to exposure control, the standard color chart with predefined reflectance values can be used [23]. Rather than using a calibration target, image-based radiometric calibration methods achieves the goal by using multiple images [35, 11, 28] or even a single image, and analyzing the RGB distributions at color edges [18], symmetric distribution of camera noise [21], geometry invariants [29] and the color properties of skin pigments [17].

Geometric calibration. To estimate the intrinsic and extrinsic parameters of a pinhole camera is indispensable in geometric computer vision. It has been achieved by using a variety of specialized calibration targets [37, 40, 43, 44] or using image information only [22, 20, 30]. Zhang's calibration method [43] is widely used in practice, because it is accurate and only requires a planar checker board. In contrast to the last generation CRT monitors, modern LCD monitors are planar. Therefore, geometric calibration using a virtual pattern [14, 42, 34, 19] is advocated, which is more convenient than making a physical checker board.

Miscellaneous applications of monitors. In addition to the use in geometric calibration, monitors have been used in radiometric calibration [39] with temporal irradiance mixture (Note that the LCD gamma characteristic is not utilized there). Multi-layer LCDs have been used for light field displays [16]. In addition, LCD monitors can be used as an ideal polarizing light source [38], because of their lighting characteristics that will be detailed in the following section.

3. Characteristics of LCD Monitors

3.1. Typical Structure of LCDs

LCD monitors are the dominant display device nowadays. The typical interior structure is illustrated in Figure 1(a). A beam of unpolarized light emits from the backboard. It goes

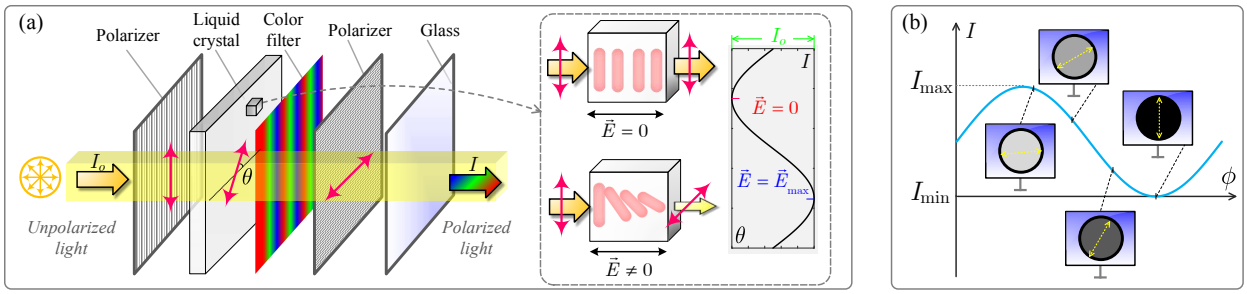

Figure 1. The principles and characteristics of LCD monitors. (a) The typical interior structure of LCD monitors. The screen brightness is controlled by adjusting the polarizing direction of the light reaching the front polarizer, yet that of transmitted light from the front polarizer keeps constant. (b) An LCD monitor viewed by a polarizing camera with different in-plane rotation angles between them.

through the first (back) linear polarizer, the liquid crystal phase retarder, and the second (front) linear polarizer, whose polarizing direction is perpendicular to that of the back polarizer. The intensity of the transmitted light is manipulated by adjusting the polarizing direction of light passing through the liquid crystal. Note that the polarization direction of the transmitted beam to the air is constant. Its intensity obeys the Malus' law

$$I = I_o \cos^2(\theta), \tag{1}$$

where θ is the rotation angle between the polarizing direction of the light passing through the liquid crystal and the transmission axis of the front polarizer; I_o is the intensity of the light from the back polarizer. When there is no voltage added to the liquid crystal layer, the rotation angle θ equals $\pi/2$, and the beam of polarized light cannot pass through the second polarizer. Otherwise, when the angle θ decreases from $\pi/2$ to 0 with increasing voltages, the intensity I will change from 0 to I_o.

3.2. LCD Monitors Viewed by a Polarizing Camera

The irradiance of a sequence of images captured by a camera with a linear polarizer rotating in front of an LCD monitor will oscillate sinusoidally between the maximum irradiance $I_{\max}$ and the minimum irradiance $I_{\min}$, as a function of the camera polarizer angle ϕ, whose function value depends on the angle difference between ϕ and the phase angle ψ of the front polarizer in the monitor (Figure 1(b)),

$$I(\phi) = \frac{I_{\max} + I_{\min}}{2} + \frac{I_{\max} - I_{\min}}{2} \cos\left[2(\phi - \psi)\right] . \tag{2}$$

Note that, Equation (2) looks the same as the reflective polarization imaging equation [15, 26, 9], which has been widely used in shape from polarization. The phase angle ψ relates to the azimuth angle of the surface normal (with some ambiguities), and the degree of polarization $\frac{I_{\max}-I_{\min}}{I_{\max}+I_{\min}}$ links to the zenith angle via the refractive index.

In our setting, there are two important characteristics that will be very helpful for camera polarizer angle calibration. First, the phase angle is related to the in-plane rotation between the camera polarizer and the monitor front polarizer.

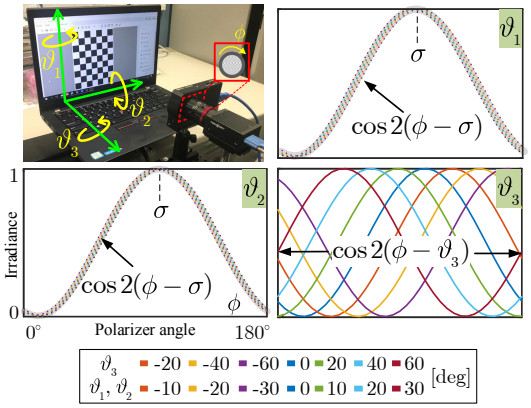

Figure 2. Illustration of transmitted radiance sinusoid (TRS) phase shift w.r.t. rotation angle ϑ_i.

Figure 2 shows how $I(\phi)$ changes when varying the rotation angles ϑ_1, ϑ_2 and ϑ_3 of the monitor along three axes respectively. It is clear that ϑ_1 or ϑ_2 is irrelevant to the phase shift in $I(\phi)$. In contrast, the monitor's in-plane rotation angle ϑ_3 plays an important role as the change in the phase angle clearly depends on ϑ_3. Therefore, we only need to estimate the monitor's in-plane rotation angle, and it is safe to ignore the other two rotations. Since the checker pattern is displayed on the monitor, the in-plane rotation between monitor (front polarizer of the monitor) and the polarizer in the camera can be easily determined by decomposing the extrinsic parameters obtained from the camera geometric intrinsic parameter and the checker pattern image. Second, the transmitted light from a modern LCD monitor is always completely polarized, so as to increase the dynamic range of the monitor, a crucial index when manufacturing LCDs. It implies that $I_{\min}$ should be close to 0 for any valid polarizer in the camera. We experimentally verified it by viewing three commodity LCD monitors at different poses using a camera with a rotating polarizer. As shown in Figure 3(a), for all configurations of monitors and poses, the ratio $I_{\min}/I_{\max}$ is less than 0.001. This property will contribute to a linear calibration method of the camera polarizer angle later.

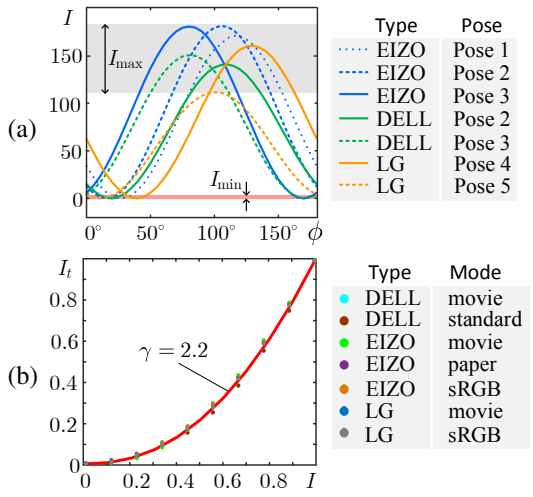

Figure 3. Illustration of LCD monitor characteristics using three commodity monitors made by EIZO, DELL and LG. (a) complete linear polarization, (b) nearly constant monitor gamma.

3.3. Gamma Characteristic of LCD Monitors

Most monitors use the *sRGB* color space mode in default. According to the IEC standards [5], the mapping between the irradiance I and the observation I^t of the *sRGB* color space can be approximated by a gamma curve of $\gamma = 2.2$. LCD monitors usually allow to change the display mode from *sRGB* to others, like *movie* and *paper*. We experimentally examined this using the three LCDs mentioned above, and our observation is shown in Figure 3(b). We can see that the monitor gamma keeps almost constant, although there are small deviations according to the monitor maker and the display mode. This characteristic will be used to obtain an initial estimate of the ICRF, and the effect of the aforementioned deviations will be largely eliminated by our bundle adjustment like operation.

4. The Proposed Method

Overview. By leveraging the characteristics of LCD monitors, our complete framework for joint radiometric and polarimetric calibration along with geometric calibration is shown in Figure 4, which consists of the following steps:

- **a)** Take several images of the adapted checker pattern on an LCD monitor from various viewpoints using a polarizing camera;
- **b)** Calibrate the camera geometric parameters using [43];
- **c)** Estimate the ICRF through a convex QP;
- **d)** Estimate the polarizer angles through a linear system using corrected observations;
- **e)** Refine the ICRF and the polarizer angles through BA.

When ICRF is known, steps **c**) and **e**) are unnecessary and the method only performs polarimetric calibration. In this special case, we can also use the standard checker pattern.

4.1. Known Inverse CRF

As mentioned in Section 3, the phase angle ψ is related to camera in-plane rotation angle directly, we can just use the yaw angle decomposed from the rotation matrix $\mathbf{R}$ as the estimation of the phase angle $\hat{\psi}$. Given the ICRF $\hat{g}$, and the estimated phase angle $\hat{\psi}$, we propose a linear solution for estimating polarizer angles. By plugging the measured intensity values $M_{k,p}$ and $\hat{g}$ into Equation (2), the relationship between the measured intensity and the polarizer angle is given by

$$\hat{g}(M_{k,p}) = t_p + a_p \cos 2(\phi_k - \hat{\psi}_p)\,, \tag{3}$$

where $t_p = (I_{\max}(p) + I_{\min}(p))/2$, $a_p = (I_{\max}(p) - I_{\min}(p))/2$ and $M_{k,p}$ is the measured intensity of the pixel p for the k-th polarizer angle ϕ_k. Recall that the transmitted light from an LCD monitor is completely polarized and $I_{\min}$ should approach 0, implying $a_p \approx t_p$. Equation (3) can be further expressed as

$$\hat{g}(M_{k,p}) = t_p\,(1 + \alpha_p \cos 2\phi_k + \beta_p \sin 2\phi_k)\,, \tag{4}$$

in which $\cos 2\phi_k$, $\sin 2\phi_k$, t_p are unknown variables and $\alpha_p = \cos 2\hat{\psi}_p$, $\beta_p = \sin 2\hat{\psi}_p$ are known values and $\hat{\psi}_p$ is the phase angle of the monitor when the pixel p is measured.

Equation (4) leads to a bilinear equation, which is hard to handle in general. Fortunately, t_p is shared for all polarizer angles and can be eliminated by dividing with the equation corresponding to the first polarizer angle:

$$\frac{\hat{g}(M_{k,p})}{\hat{g}(M_{1,p})} = \frac{1 + \alpha_p \cos 2\phi_k + \beta_p \sin 2\phi_k}{1 + \alpha_p \cos 2\phi_1 + \beta_p \sin 2\phi_1}\,, \tag{5}$$

for $k = 2, \ldots, K$ and $p = 1, \ldots, P$, where K and P represent the number of polarizer angles and that of pixels, respectively. Note that it assumes $\hat{g}(M_{1,p}) \neq 0$, *i.e.*, $t_p \neq 0$ and it implies $\phi_1 \neq \hat{\psi}_p \pm \pi/2$.

By cross multiplication, Equation (5) becomes a linear equation, which can be stacked into a matrix form

$$\tilde{\mathbf{D}} = \tilde{\mathbf{O}}\tilde{\mathbf{P}}\,, \tag{6}$$

with

$$\tilde{\mathbf{O}} = \begin{bmatrix} \mathbf{p}_2 & -\mathbf{p}_1 & \mathbf{0} & \ldots & \mathbf{0} \\ \mathbf{p}_3 & \mathbf{0} & -\mathbf{p}_1 & \ldots & \mathbf{0} \\ \vdots & \vdots & \vdots & \ddots & \vdots \\ \mathbf{p}_K & \mathbf{0} & \mathbf{0} & \ldots & -\mathbf{p}_1 \end{bmatrix}, \quad \tilde{\mathbf{P}} = \begin{bmatrix} \cos 2\phi_1 \\ \sin 2\phi_1 \\ \vdots \\ \cos 2\phi_K \\ \sin 2\phi_K \end{bmatrix},$$

and

$$\tilde{\mathbf{D}} = \big[\hat{I}_{1,1} - \hat{I}_{2,1}, \quad \ldots, \quad \hat{I}_{1,P} - \hat{I}_{2,P}, \quad \ldots, \\ \hat{I}_{1,1} - \hat{I}_{K,1}, \quad \ldots, \quad \hat{I}_{1,P} - \hat{I}_{K,P}\big]\,.$$

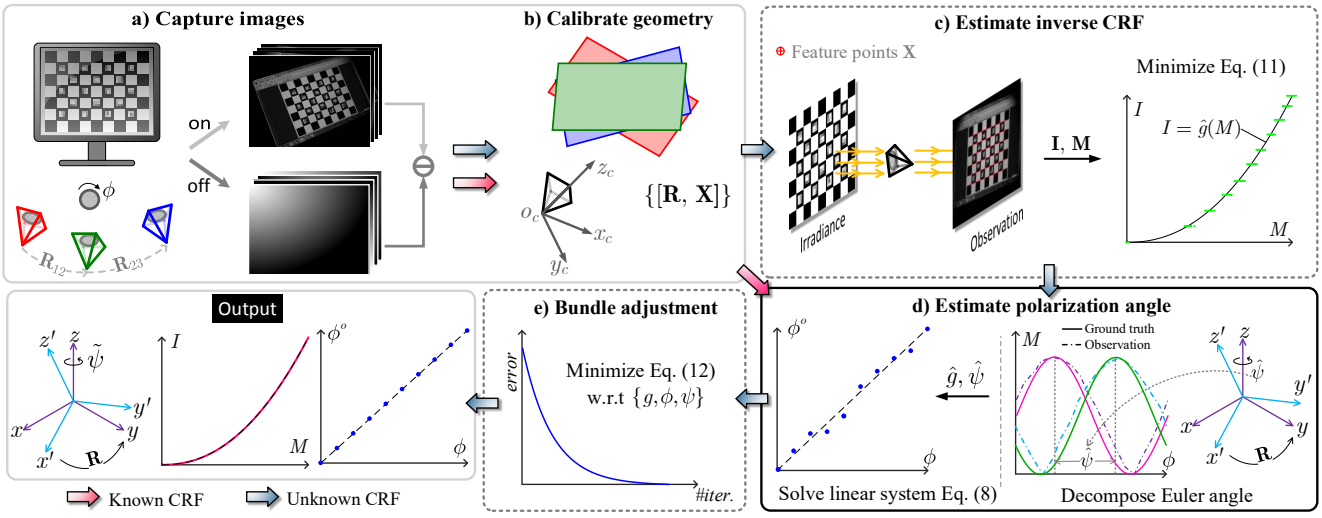

Figure 4. The flowchart of the proposed method. By taking a few images of the gamma compensated checker pattern displayed on an LCD screen, we use Zhang's method for geometric calibration. The ICRF is calibrated using patches with linear radiance. Using the corrected profiles, the camera polarizer angles are calibrated by solving a linear system with the assistance of extrinsic pose decomposition. A bundle adjustment like procedure is used to further refine the estimated ICRF and polarizer angles jointly.

The submatrix $\mathbf{p}_m$ can be constructed by

$$\mathbf{p}_m = \begin{bmatrix} \alpha_1 \hat{I}_{m,1} & \alpha_2 \hat{I}_{m,2} & \cdots & \alpha_P \hat{I}_{m,P} \\ \beta_1 \hat{I}_{m,1} & \beta_2 \hat{I}_{m,2} & \cdots & \beta_P \hat{I}_{m,P} \end{bmatrix}^T, \quad (7)$$

and $\hat{I}_{m,p} = \hat{g}(M_{m,p})$ for $m = 1, \ldots, K$. Hence, we can solve the linear system easily as

$$\tilde{\mathbf{P}} = \left(\tilde{\mathbf{O}}^T \tilde{\mathbf{O}}\right)^{-1} \tilde{\mathbf{O}}^T \tilde{\mathbf{D}}, \quad (8)$$

from which the polarizer angles ϕ_k can be obtained. This linear method to calibrate the angles is one of the key features of the proposed method, since it does not require any iteration and initialization.

According to Equation (4), the number of constraints is KP, which should be no less than the number of variables $K+P$, *i.e.*, $KP \geq K+P$. This gives the minimal requirements for our calibration method. Specifically, we need that $K \geq 2$ and $P \geq 2$, that is, our method applies to a polarizing camera with two or more polarizing channels. Considering that all pixels of the screen have the same phase shift, $P \geq 2$ implies that the LCD monitor (or the camera) should rotate at least once in the polarizer plane. In other words, our method is degenerate if no in-plane rotation happens in all poses. Note that this case is not degenerate for Zhang's geometric calibration method. However, we believe this requirement imposes little restriction in practice.

4.2. Unknown Inverse CRF

Calibration pattern. When the ICRF is unknown, we calibrate it by leveraging the characteristics of LCD monitors.

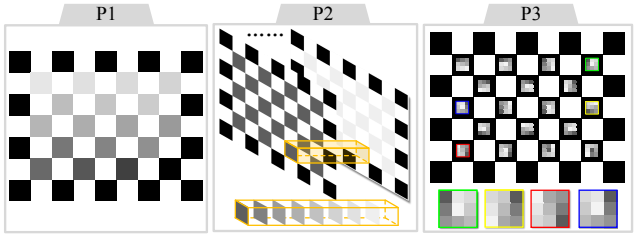

Figure 5. Calibration patterns.

We designed three patterns (Figure 5): P1, which is more similar to the standard checker; P2, which consists of a sequence of dithered B/W patterns; and P3, our adapted checker pattern. P3 is based on a 7×9 checkerboard and each inner dark square contains 3×3 small patches. The intensity of the surrounding dark areas is set to 0, so as to facilitate corner detection for the geometric calibration algorithm [43]. To compensate the gamma characteristic of LCDs, the 3×3 patches are pre-corrected using $I_t = A I_o^{1/\gamma}$, with I_o equals $[0.1, 0.2, \ldots, 0.9]$ and A equals 255. We have observed *spatial inconsistency* when the camera is tilted away from the LCD monitor. This is because the observed intensities of the same screen point will change according to the viewing directions. We thus use small patches and take the average for the same patches in all squares to alleviate this effect.

Inverse CRF estimation. The ICRF can be approximated by a polynomial expression [24]

$$I = g(M) = \sum_{n=0}^{N} c_n M^n, \quad (9)$$

where M and I denote the measured intensity and the corresponding irradiance, respectively. c_n are the coefficients and N is the order of the polynomial. For the reason that the irradiance and the measured intensity are normalized in the range of $[0, 1]$, the constraints $g(0)=0$ and $g(1)=1$ are needed. Additionally, the ICRF of a real-world camera is usually smooth and monotonically increasing. Therefore the space $\mathcal{W}$ of ICRFs is defined as [13]

$$\mathcal{W} := \{g \mid g(0) = 0, g(1) = 1, \partial g/\partial M > 0\} \ . \quad (10)$$

Thanks to our gamma corrected checker pattern, the ICRF estimation can be simply achieved by solving the following convex quadratic program

$$\hat{g} = \underset{g \in \mathcal{W}}{\operatorname{argmin}} \|\mathbf{I} - g(\mathbf{M})\|^2 + \lambda |\frac{\partial^2 g}{\partial M^2}|, \quad (11)$$

where $\mathbf{I}$ denotes the stacked linear irradiance in matrix form, and $\mathbf{M}$ the stacked observations. λ is a weighting factor, which is fixed to 0.001.

Polarizer angle estimation. After recovering the ICRF, the method described in Section 4.1 can be used to estimate polarizer angles.

Bundle adjustment. As shown in Figure 3(b), the monitor gamma might slightly deviate from 2.2. The consequence is that the ICRF estimation and the subsequent angle estimation might be inaccurate. To account for this issue, we propose to jointly refine the ICRF and the polarizer angles, by using nonlinear optimization similar to bundle adjustment. We minimize the following cost function

$$\sum_{k=1}^{K} \sum_{p=1}^{P} \|t_p \left(c(2\phi_k)c(2\psi_p) + s(2\phi_k)s(2\psi_p) + 1\right) - g(M_{k,p})\|^2 \ , \quad (12)$$

where $c(\cdot)$ and $s(\cdot)$ denote $\cos(\cdot)$ and $\sin(\cdot)$ respectively. We use the `fmincon` function in Matlab for minimization, which is initialized by using the estimated ICRF $\hat{g}$, phase angle $\hat{\psi}$, and polarizer angles $\hat{\phi}$.

Note that the validity of the objective function in Equation (12) does not rely on the monitor gamma, even if it is different from 2.2. The monitor gamma can affect the initialization only.

5. Experiments

5.1. Simulation

We first conduct experiments based on the synthetic data, to validate our method. The synthetic data are generated using 201 inverse CRFs from the database [12]. A zero-mean Gaussian noise $\mathcal{N}(0, \sigma^2)$ with $\sigma = 2$ is added. The root mean square error (RMSE) is used as evaluation metrics.

Known inverse CRF. When the ICRF is given, we can compare our method with Schechner's method [32] directly. For Schechner's method [32], we use random initialization of the angles. We run these two methods 100 times. Different numbers of polarizing channels are tested ($K=18$ and $K=4$) for validating how the number of channels affect the methods' performance. Figure 6(a-b) shows the results. We found that 1) our method performs well and the result is close to the ground truth. 2) Schechner's method is sensitive to initialization, but our method doesn't suffer from this problem. 3) Schechner's method is less reliable when the number of angles is small while ours is still robust.

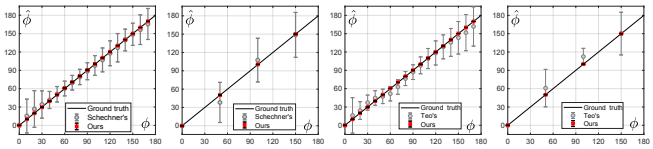

(a) 18 polar. angles (b) 4 polar. angles (c) 18 polar. angles (d) 4 polar. angles

Figure 6. Results from 100 independent trials, for 18 and 4 polarization angles, (a-b) known ICRF, (c-d) unknown ICRF.

Unknown inverse CRF. We apply our method and Teo's method [36] to these synthetic data to estimate the polarizer angles along with the ICRF. We obtain that using our method, the RMSE of mean angles is about 0.18/0.09 degrees for $K=18$ and $K=4$. For Teo's method, the RMSE of mean angles and mean of std. are as high as 5.18/8.26 and 17.10/19.79, respectively (Figure 6(c-d)). We observe that this high error is due to the camera response nonlinearity in the data and random initialization. Teo's method [36] often requires a near ground truth initial guess to work well.

Sensitivity analysis. We conduct thorough sensitivity analysis to assess the performance (angular RMSE) as a function of the noise std. (Figure 7). We observe that 1) Schechner's method is not sensitive to noise, but to initialization. 2) Our linear method is sensitive to large noise. 3) Our joint method can suppress noise effectively.

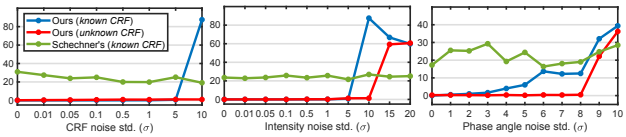

Figure 7. Sensitivity to the noise standard deviation (σ).

5.2. Real-world Experiments

Experiment setup. For real experiments, we use a Point-Grey GS3-U3-15S5M-C grayscale camera and a polarizer in the visible range (SIGMA KOKI SPF-30C-32) to capture images. An accurate mechanical rotator is used to obtain the ground truth of the polarizer angles. The Thinkpad T470S is used as the LCD monitor in experiments, with another mechanical rotator equipped for rotating it.

Environment illumination. The real-world data is divided into two categories. One is captured in a dark room without

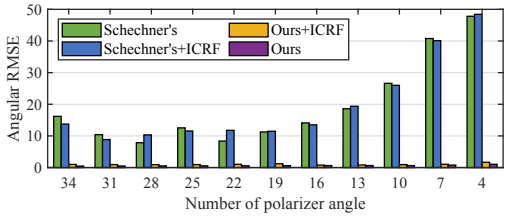

Figure 8. Comparison of different numbers of polarizer angles.

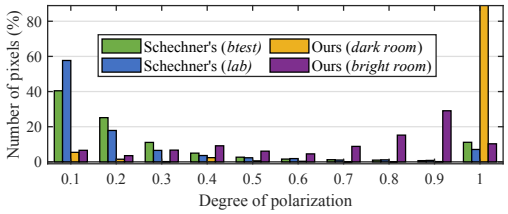

Figure 9. Distribution of degree of polarization (DoP).

the influence of environment illumination (*dark room* data). The other is captured under the environment illumination (*bright room* data). To address environment illumination in the bright room data, we capture images when the monitor is switched off and subtract them from input data. Table 1 shows the results of applying our method to the *dark room* and *bright room* data respectively. We can find that the effect of environmental illumination can be reliably removed via subtraction, and our method can achieve good results. In addition, by estimating ICRF simultaneously, the polarizer angles can be estimated more accurately since the given ICRF could contain errors.

Table 1. Results under different environment illumination settings.

	Known ICRF		Unknown ICRF	
	CRF err.	Ang. err.	CRF err.	Ang. err.
Dark room	✗	0.76 ± 0.20	0.01 ± 0.01	$\mathbf{0.48\pm0.15}$
Bright room	✗	0.80 ± 0.28	0.05 ± 0.01	$\mathbf{0.71\pm0.11}$

Effectiveness of using less polarizer angles. Figure 8 presents the comparison of different numbers of polarizer angles. Our method is robust with the decrease in the number of polarizer angles, while Schechner's method becomes less reliable with fewer polarizer angles.

Effectiveness of point selection. Previous polarization calibration methods [32, 36] are image-based self-calibration methods. They all require carefully selected pixels. Our method benefits from the use of LCD monitors. 1) Polarization characteristics of LCD monitors provide us a good source of polarization. 2) The adapted checker pattern gives us infomation on feature points. It is easy for us to choose valid points. We compute the distribution of DoP in [32] released data (*i.e.*, *btest* and *lab*) with our *dark room* and *bright room* data. Figure 9 shows the results.

Benefits of the adapted checker pattern P3. Table 2 compares patterns and shows that when ICRF is known the standard checker pattern can achieve the same accuracy. When ICRF is unknown, the proposed joint calibration approach can obtain estimates very close to the ground truth. P1 suffers from *spatial inconsistency* and is less reliable. The result using P2 could be more accurate. However, it would require more images. In addition, the accurate estimated ICRF could be distorted during BA process for reducing polarizer angle errors. P3 gives results close to P2 but with less images.

Table 2. Comparison of different patterns (P0: *Checkerboard*).

	Known ICRF			Unknown ICRF		
	CRF err.	Ang. err.	#images	CRF err.	Ang. err.	#images
P0	✗	0.80 ± 0.16	≥ 4	0.20 ± 0.06	82.2 ± 26.1	≥ 4
P1	✗	0.78 ± 0.15	≥ 4	0.07 ± 0.02	1.24 ± 0.43	≥ 4
P2	✗	0.79 ± 0.14	≥ 4	0.02 ± 0.02	$\mathbf{0.38\pm0.32}$	$\geq 4+11$
P3	✗	0.78 ± 0.15	≥ 4	$\mathbf{0.01\pm0.01}$	0.48 ± 0.15	≥ 4

Joint calibration *vs*. separate calibration. It is possible to conduct the polarization calibration and the CRF calibration separately. In this case, our proposed method will still be very useful. For example, when the ICRF is given, our linear polarization calibration method can be used. When the ICRF is unknown, it is possible to calibrate it by developing a separate method (in Table 3, we put the separately estimated CRF using P2 and phase angle using P0 into our linear method). Yet, our finding is that the use of P3 will give a rough calibration of the camera response, and linking camera radiometric calibration with polarization calibration through bundle adjustment will greatly improve the accuracy of both. The cost to pay is very small here, since the image capture process is completely the same as in pure geometric calibration. With the proposed estimation method and bundle adjustment step, experiments (Table 3) show that our calibration results are very close to the ground truth, indicating that joint calibration is both effective and efficient. The calibration efficiency is crucial in many scenarios. We thus believe our joint calibration method can be a convenient and integrated tool for polarizing imaging.

Table 3. Comparison of separate and joint processes.

	Known ICRF				Unknown ICRF			
	CRF err.	Ang. err.	ψ err.	#images	CRF err.	Ang. err.	ψ err.	#images
Separate	✗	0.45	3.08	$\geq 4+2$	0.02	0.83	3.10	$\geq 4+2+11$
Joint	0.02	**0.38**	**0.19**	$\geq \mathbf{4}$	**0.01**	**0.48**	**0.20**	$\geq \mathbf{4}$

Comparison with the state-of-the-art methods. We compare our method with the state-of-the-art methods [32, 36] using real images (*bright room* data). Figure 10 presents the comparison results. We can observe that our method has the best performance in polarizer angle estimation. In addition, it gives an accurate estimation of ICRF. When the ICRF is not given, Schechner's method fed with a CRF estimated using P2 performs poorly. If the ICRF is given, its performance becomes much better, but still worse than ours,

due to occasional poor convergence from random initialization. We observe Schechner's method often suffers from the problem that the estimated angles are perpendicular to ground truth. For fair comparison, we reverse manually its results when necessary. Teo's method [36] is an image-based self-calibration method. It gives a rough estimation of ICRF, but the involvement of ICRF estimation makes their results worse. It is also sensitive to initialization.

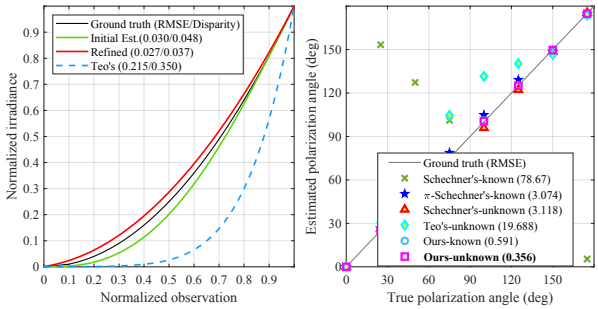

CRF	Method	CRF err.	Ang. err.	#polar. ang.	#images
known	[32]	✗	8.85 ± 15.39	≥ 4	≥ 4
	Ours	✗	$\mathbf{0.62\pm0.28}$	$\geq \mathbf{2}$	≥ 4
unknown	[32] + ICRF	✗	15.84 ± 29.59	≥ 4	$\geq 4+11$
	[36]	0.13 ± 0.09	12.56 ± 7.31	≥ 4	≥ 4
	Ours	$\mathbf{0.04\pm0.02}$	$\mathbf{0.63\pm0.18}$	$\geq \mathbf{2}$	≥ 4

Figure 10. Comparison with state-of-the-art methods.

6. Discussions

Applicability. For cameras with a mosaicing polarization array, the polarizer angle is fixed and known beforehand. Thus, polarization calibration for such cameras is basically unnecessary. However, such cameras have well-known issues of strong cross-talks between different channels and spatial nonuniformness. So, we believe that rotating a polarizer by hand in front of a fixed camera will still be a common practice in low-cost polarizing imaging, for which our calibration method is very useful. For high-quality polarizing imaging of dynamic scenes, the multi-sensor solution will still be indispensable. It is sometimes desirable to adjust the polarizing angles according to the target. The Spectral Devices Inc. released such a multi-sensor camera system [4], which allows users to insert proper polarizing filters according to their specific applications. It will arouse the need of radiometric and polarimetric calibration very frequently, since it is hard to exactly control the filter's angle when inserting it into the camera.

LCD screens with a touch panel. LCD screens on most mobile devices, such as cell phones, are equipped with a touch panel on top of the front polarizer. We have examined its effect by using a rotating polarizer. As shown in Figure 11, three cell phones, including a HUAWEI Mate 10 Lite, an Apple iPhone 6s and an Apple iPhone 7 Plus, were tested. The HUAWEI Mate 10 Lite screen (a) functions in the same way as a desktop LCD monitors, and can be used as the calibration target. On the contrary, although the iPhone 6s screen (b) has no spatially varying phase shift, the emitted light is not completely polarized. The iPhone 7 Plus screen (c) exhibits obvious color change and spatially varying phase shift, as the polarizer rotates. Therefore, both can not be used for our calibration task. To play safe, we recommend to use a desktop or laptop monitors without a touch panel for the calibration task.

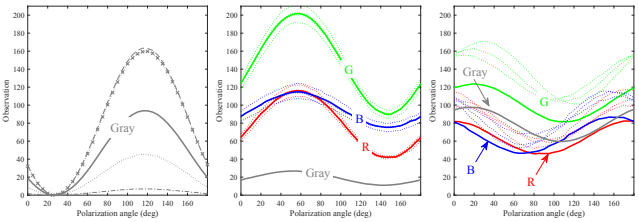

(a) HUAWEI Mate 10 Lite (b) iPhone 6s (c) iPhone 7 Plus

Figure 11. Cell phones' screen characteristic.

Environment illumination. When the monitor is facing the glass window or the ceiling lamp directly, we have observed mixed polarizing light from the LCD monitor (active) and the screen reflection (passive). Considering that the active monitor light can be easily switched off, a simple subtraction method of the environment background has been proven effective. Instead of subtraction, the screen could cause reflective polarization, which is related to the azimuth angle of the normal perpendicular to the screen (or the front polarizer). We will explore how to model this mixture in our future work.

7. Conclusion

In this paper, we have proposed to jointly calibrate the camera response function and the polarizer angles of a polarizing camera by viewing an adapted checker pattern displayed on an LCD monitor. The image capturing operation is very similar to that in geometric camera calibration using a 2D checker pattern, except for the mild requirement that at least one view has in-plane rotation against the others. By leveraging the gamma characteristic, the radiometric calibration can be easily conducted through a convex program. Thanks to the lighting principles of LCD monitors and the extrinsic parameters from geometric calibration, our calibration method for polarizer angles is linear. The initial estimates can be jointly improved through a bundle adjustment like operation. Experiment results have verified the accuracy and reliability of our proposed calibration method. Considering that LCD monitors are everywhere, we believe our method will facilitate polarimetric imaging.

Acknowledgments. This work was finished when Zhixiang Wang visited the Optical Sensing and Camera System Laboratory (Oscars Lab), led by Dr. Yinqiang Zheng at National Institute of Informatics (NII), Japan, through the NII International Internship Program.

References

[1] 4D technology polarization camera. https://www.4dtechnology.com/products/polarimeters/polarcam/.

[2] FluxData polarization camera. http://www.fluxdata.com/imaging-polarimeters.

[3] Phoenix polarization camera. https://thinklucid.com/phoenix-machine-vision/.

[4] Spectral multi-sensor camera system. https://www.spectraldevices.com/products/multi-camera-imaging-systems.

[5] Matthew Anderson, Ricardo Motta, Srinivasan Chandrasekar, and Michael Stokes. Proposal for a standard default color space for the InternetsRGB. In *Color and Imaging Conference*, 1996.

[6] Gary A. Atkinson and Edwin R. Hancock. Recovery of surface orientation from diffuse polarization. *IEEE Transactions on Image Processing*, 15(6):1653–1664, 2006.

[7] Kai Berger, Randolph Voorhies, and Larry H. Matthies. Depth from stereo polarization in specular scenes for urban robotics. In *Proceedings of International Conference on Robotics and Automation (ICRA)*, 2017.

[8] Edward Collett. *Field Guide to Polarization*, volume 15. SPIE Press, 2005.

[9] Zhaopeng Cui, Jinwei Gu, Boxin Shi, Ping Tan, and Jan Kautz. Polarimetric multi-view stereo. In *Proceedings of Conference on Computer Vision and Pattern Recognition (CVPR)*, 2017.

[10] Paul E. Debevec and Jitendra Malik. Recovering high dynamic range radiance maps from photographs. In *Proceedings of ACM SIGGRAPH*, 1997.

[11] Mauricio Díaz and Peter Sturm. Radiometric calibration using photo collections. In *Proceedings of International Conference on Computational Photography (ICCP)*, 2011.

[12] Michael D. Grossberg and Shree K. Nayar. What is the space of camera response functions? In *Proceedings of Conference on Computer Vision and Pattern Recognition (CVPR)*, 2003.

[13] Michael D. Grossberg and Shree K. Nayar. Modeling the space of camera response functions. *IEEE Transactions on Pattern Analysis and Machine Intelligence*, 26(10):1272–1282, 2004.

[14] Hyowon Ha, Yunsu Bok, Kyungdon Joo, Jiyoung Jung, and In So Kweon. Accurate camera calibration robust to defocus using a smartphone. In *Proceedings of International Conference on Computer Vision (ICCV)*, 2015.

[15] Achuta Kadambi, Vage Taamazyan, Boxin Shi, and Ramesh Raskar. Depth sensing using geometrically constrained polarization normals. *International Journal of Computer Vision*, 125(1-3):34–51, 2017.

[16] Douglas Lanman, Gordon Wetzstein, Matthew Hirsch, Wolfgang Heidrich, and Ramesh Raskar. Polarization fields: dynamic light field display using multi-layer LCDs. *ACM Transactions on Graphics*, 30(6):186, 2011.

[17] Chen Li, Stephen Lin, Kun Zhou, and Katsushi Ikeuchi. Radiometric calibration from faces in images. In *Proceedings of Conference on Computer Vision and Pattern Recognition (CVPR)*, 2017.

[18] Stephen Lin, Jinwei Gu, Shuntaro Yamazaki, and Heung-Yeung Shum. Radiometric calibration from a single image. In *Proceedings of Conference on Computer Vision and Pattern Recognition (CVPR)*, 2004.

[19] Yuankun Liu and Xianyu Su. Camera calibration with planar crossed fringe patterns. *Optik-International Journal for Light and Electron Optics*, 123(2):171–175, 2012.

[20] Quang-Tuan Luong and Olivier D. Faugeras. Self-calibration of a moving camera from point correspondences and fundamental matrices. *International Journal of Computer Vision*, 22(3):261–289, 1997.

[21] Yasuyuki Matsushita and Stephen Lin. Radiometric calibration from noise distributions. In *Proceedings of Conference on Computer Vision and Pattern Recognition (CVPR)*, 2007.

[22] Stephen J. Maybank and Olivier D. Faugeras. A theory of self-calibration of a moving camera. *International Journal of Computer Vision*, 8(2):123–151, 1992.

[23] C. S. McCamy, H. Marcus, and J. G. Davidson. A color-rendition chart. *Journal of Applied Photographic Engineering*, 2(3):95–99, 1976.

[24] Tomoo Mitsunaga and Shree K. Nayar. Radiometric self calibration. In *Proceedings of Conference on Computer Vision and Pattern Recognition (CVPR)*, 1999.

[25] Daisuke Miyazaki, Masataka Kagesawa, and Katsushi Ikeuchi. Transparent surface modeling from a pair of polarization images. *IEEE Transactions on Pattern Analysis and Machine Intelligence*, 26(1):73–82, 2004.

[26] Daisuke Miyazaki, Takuya Shigetomi, Masashi Baba, Ryo Furukawa, Shinsaku Hiura, and Naoki Asada. Surface normal estimation of black specular objects from multiview polarization images. *Optical Engineering*, 56(4):041303, 2016.

[27] Daisuke Miyazaki, Robby T. Tan, Kenji Hara, and Katsushi Ikeuchi. Polarization-based inverse rendering from a single view. In *Proceedings of International Conference on Computer Vision (ICCV)*, 2003.

[28] Zhipeng Mo, Boxin Shi, Sai-Kit Yeung, and Yasuyuki Matsushita. Radiometric calibration for internet photo collections. In *Proceedings of Conference on Computer Vision and Pattern Recognition (CVPR)*, 2017.

[29] Tian-Tsong Ng, Shih-Fu Chang, and Mao-Pei Tsui. Using geometry invariants for camera response function estimation. In *Proceedings of Conference on Computer Vision and Pattern Recognition (CVPR)*, 2007.

[30] Marc Pollefeys, Reinhard Koch, and Luc Van Gool. Self-calibration and metric reconstruction inspite of varying and unknown intrinsic camera parameters. *International Journal of Computer Vision*, 32(1):7–25, 1999.

[31] Megumi Saito, Yoichi Sato, Katsushi Ikeuchi, and Hiroshi Kashiwagi. Measurement of surface orientations of transparent objects using polarization in highlight. In *Proceedings of Conference on Computer Vision and Pattern Recognition (CVPR)*, 1999.

[32] Yoav Y. Schechner. Self-calibrating imaging polarimetry. In *Proceedings of International Conference on Computational Photography (ICCP)*, 2015.

[33] William A. P. Smith, Ravi Ramamoorthi, and Silvia Tozza. Linear depth estimation from an uncalibrated, monocular polarisation image. In *Proceedings of European Conference on Computer Vision (ECCV)*, 2016.

[34] Zhan Song and Ronald Chung. Use of LCD panel for calibrating structured-light-based range sensing system. *IEEE Transactions on Instrumentation and Measurement*, 57(11):2623–2630, 2008.

[35] Jun Takamatsu and Yasuyuki Matsushita. Estimating camera response functions using probabilistic intensity similarity. In *Proceedings of Conference on Computer Vision and Pattern Recognition (CVPR)*, 2008.

[36] Daniel Teo, Boxin Shi, Yinqiang Zheng, and Sai-Kit Yeung. Self-calibrating polarising radiometric calibration. In *Proceedings of Conference on Computer Vision and Pattern Recognition (CVPR)*, 2018.

[37] Roger Tsai. A versatile camera calibration technique for high-accuracy 3D machine vision metrology using off-the-shelf TV cameras and lenses. *IEEE Journal on Robotics and Automation*, 3(4):323–344, 1987.

[38] Gordon Wetzstein, Wolfgang Heidrich, and David Luebke. Optical image processing using light modulation displays. *Computer Graphics Forum*, 29(6):1934–1944, 2010.

[39] Bennett Wilburn, Hui Xu, and Yasuyuki Matsushita. Radiometric calibration using temporal irradiance mixtures. In *Proceedings of Conference on Computer Vision and Pattern Recognition (CVPR)*, 2008.

[40] Xianghua Ying and Hongbin Zha. Geometric interpretations of the relation between the image of the absolute conic and sphere images. *IEEE Transactions on Pattern Analysis and Machine Intelligence*, 28(12):2031–2036, 2006.

[41] Ye Yu, Dizhong Zhu, and William A. P. Smith. Shape-from-polarisation: a nonlinear least squares approach. In *Proceedings of International Conference on Computer Vision (ICCV)*, 2017.

[42] Zongqian Zhan. Camera calibration based on liquid crystal display (LCD). *The International Archives of the Photogrammetry, Remote Sensing and Spatial Information Sciences*, 37(1), 2008.

[43] Zhengyou Zhang. A flexible new technique for camera calibration. *IEEE Transactions on Pattern Analysis and Machine Intelligence*, 22(11):1330–1334, 2000.

[44] Zhengyou Zhang. Camera calibration with one-dimensional objects. *IEEE Transactions on Pattern Analysis and Machine Intelligence*, 26(7):892–899, 2004.